PERGAMON

Chemical Engineering Science 55 (2000) 4423–4434

Chemical Engineering Science

A large eddy PIV method for turbulence dissipation rate estimation

J. Sheng[a,b], H. Meng[a,c], R. O. Fox[a,d,*]

[a]*Program for Complex Fluid Flows, Kansas State University, USA*
[b]*Department of Mechanical Engineering, Johns Hopkins University. Baltimore, MD 21218, USA*
[c]*Department of Mechanical and Aerospace Engineering, SUNY at Buffalo, Buffalo, NY 14260-4400, USA*
[d]*Department of Chemical Engineering, Iowa State University, Ames, IA 50011-2230, USA*

Received 14 October 1997; accepted 14 January 2000

Abstract

Accurate estimation of the turbulence dissipation rate is important for the turbulent flows in the chemical process industry. Previous studies, limited by single-point velocity measurement techniques, mainly focus on measuring the single-point local dissipation rate or averaged dissipation rate over a finite volume. Various methods — turbulent kinetic energy balance, Taylors hypothesis, and dimensional analysis — have been proposed to estimate the dissipation rate of turbulent kinetic energy. These methods cannot provide the global distribution of the dissipation rate over a large flow region. Since particle image velocimetry (PIV) is capable of providing multi-point instantaneous measurements of a flow field, it is more suitable for examining the dissipation rate distribution. However, PIV measurements are limited to finite grid sizes, which often exceed the smallest eddy sizes that dominate the turbulence dissipation rate. In this paper, a large eddy PIV method for dissipation rate estimation is proposed. Based on a dynamic-equilibrium assumption for the sub-grid scale (SGS) flux between the resolved and the sub-grid scales, our method measures the SGS energy flux, and thus, estimates the turbulence dissipation rate. The SGS flux is obtained from the strain-rate tensors computed from velocity fields and the modeled SGS stress. When the PIV measurement resolves down to the Kolmogorov scale, the SGS stress is replaced with the viscous shear stress. In other words, the resolved velocity fields directly give the dissipation rate. This method is applied to estimate the dissipation rate along the center plane of a stirred vessel with an axial 45° pitched-blade turbine. The results obtained are compared with those calculated using the dimensional analysis method. The average dissipation rates over the impeller and flow discharge regions are also evaluated and compared using both methods.

Keywords: Turbulence; Dissipation rate; Particle image velocimetry; Large eddy simulation; Stirred vessel

1. Introduction

Turbulent flows contain eddy motions of a wide range of time and length scales and hence are often used in the chemical process industry to promote macro- and micro-mixing and chemical reaction. The dissipation rate of turbulent kinetic energy determines the degree of segregation, droplet and bubble break-down, and chemical reaction. Therefore, it is important to know the dissipation rate over the entire flow field. Various methods have been proposed for estimating the turbulence dissipation rate. Limited by single-point velocity measurement techniques, previous studies mainly focus on measuring the single-point local dissipation rate or averaged dissipation rate over a finite volume. In what follows, we briefly review existing methods for estimating the turbulence dissipation rate.

1.1. Review of methods of dissipation rate estimation

1.1.1. Direct measurement of strain rate tensors

Direct approximation from the definition,

$$\varepsilon = 2\upsilon\langle s'_{ij}\, s'_{ij}\rangle = \frac{\upsilon}{2}\left\langle\left(\frac{\partial u'_i}{\partial x_j} + \frac{\partial u'_j}{\partial x_i}\right)^2\right\rangle, \tag{1}$$

where u'_i is the ith component of the fluctuating velocity, requires highly resolved turbulence fluctuating strain-rate fields. So far, only three-dimensional numerical simulation (direct numerical simulation, or DNS) can provide full-field estimation of the dissipation rate. Single-point measurements in a wind tunnel have been

* Corresponding author. Tel.: 001-515-294-9104; fax: 001-515-294-2689.
E-mail address: rofox@iastate.edu (R. O. Fox).

0009-2509/00/$ - see front matter
PII: S0009-2509(00)00039-7

conducted using nine spatially aligned hot-wire probes (Andreopoulos & Honkan, 1996). However, in order to resolve the strain rate field, the spatial resolution has to be smaller than Kolmogorov length scale, and only multiple hot-wire probes are known to meet this requirement. Such intrusive complex probes are generally unsuitable for complex flows common to the chemical process industry.

1.1.2. Turbulent kinetic energy balance

In this approach, the turbulence dissipation rate is approximated by inverting the stationary turbulent kinetic energy balance equation, i.e.,

$$\varepsilon = \langle U_j \rangle \frac{\partial k}{\partial x_j} + \frac{\partial}{\partial x_j}(\langle p u_j' \rangle + 2\mu \langle u_j' s_{ij}' \rangle + \tfrac{1}{2}\langle u_i' u_j'^2 \rangle) + \langle u_i' u_j' \rangle \frac{\partial U}{\partial x_j}. \quad (2)$$

This approach requires experimental evaluation of all the right-hand-side terms, which involve only integral-scale turbulence quantities. Hussein and Martinuzzi (1995) have successfully applied this method for estimating the dissipation rate along the center plane of a channel flow passing over a surface mounted cube using point-wise LDV measurements. However, it is clear that without a dependable velocimetry tool capable of measuring 3D volumetric velocity fields, it will be very difficult to obtain the required spatial derivatives across a large measurement area. Thus, certain assumptions have to be adopted to simplify the equation to 2D, or even 1D. Furthermore, the pressure and velocity correlation term, $\langle p' u_i' \rangle$, is difficult to measure directly from experiments, and models or assumptions must be applied, such as assuming a zero-pressure–velocity correlation (Landahl & Mollo-Christensen, 1992). These difficulties limit the methods applicability to simple geometries, and hence make it unsuitable for estimating the turbulence dissipation rate in process equipment.

1.1.3. Turbulence power spectrum

In homogeneous turbulence, the local dissipation rate can be defined in terms of the energy spectrum, $E(\kappa, t)$:

$$\varepsilon = 2\upsilon \int_0^4 \kappa^2 E(\kappa, t)\, \mathrm{d}\kappa. \quad (3)$$

For isotropic turbulence, it can be written as

$$\varepsilon = 15\upsilon \int \kappa_1^2 E_1(\kappa_1)\, \mathrm{d}\kappa_1, \quad (4)$$

where $E_1(\kappa_1)$ is the one-dimensional power spectrum. In theory, by measuring $E_1(\kappa_1)$, the turbulence dissipation rate can be approximated from Eq. (4). However, in order to fully resolve $E_1(\kappa_1)$, the velocity measurements must be sampled at a rather high frequency. Unfortunately, current hot-wire probes and LDV often do not extend to high enough wave numbers to allow the application of this method for process equipment.

1.1.4. Taylor's frozen turbulence hypothesis

It assumes that the turbulent eddies are advected past the point of observation by the mean flow fast enough so that they do not have time to change substantially during the time of passage. In this way, spatial derivatives can be approximated by time derivatives. Therefore, the spatial covariance needed to evaluate the turbulence dissipation rate can be determined from time covariance using the following relationship:

$$\left\langle \left(\frac{\partial u_i'}{\partial x_i} \right)^2 \right\rangle = \frac{1}{\bar{U}_1^2} \left\langle \left(\frac{\partial u_i'}{\partial t} \right)^2 \right\rangle. \quad (5)$$

For isotropic homogeneous turbulence, the dissipation rate can, therefore, be expressed in terms of the time covariance (Hinze, 1994)

$$\varepsilon = \frac{15\upsilon}{\bar{U}^2} \left\langle \left(\frac{\partial u_1}{\partial t} \right)^2 \right\rangle. \quad (6)$$

This relationship is based on the assumption that the principal direction of flow is with the chosen coordinate axes, and that the turbulence intensity is low. These conditions do not hold for complex flows like stirred tanks (van Doorn, 1981). When applying this method, care must be taken to validate the frozen turbulence assumption. In practice, LDV sampling limitations often make such validation impossible.

1.1.5. Dimensional analysis

In isotropic turbulence, the turbulence dissipation rate can be expressed in terms of a micro-scale and the turbulence velocity fluctuations

$$\varepsilon = 15\upsilon \frac{u'^2}{\lambda^2}, \quad (7)$$

where λ is the Taylor micro-scale. Alternatively, using equilibrium turbulence arguments (Batchelor, 1953; Tennekes & Lumley, 1972) Eq. (7) can be re-expressed as

$$\varepsilon = A \frac{u'^3}{l}, \quad (8)$$

where l is the integral length scale and A is a proportionality constant of order 1. In theory, Eq. (8) applies only to turbulence that is homogeneous, isotropic, and in spectral equilibrium, but in practice, it is rather difficult to meet these conditions. Moreover, in the complex flows, e.g., the flow in a stirred tank, the integral length scale varies from region to region. Thus, a single value for l cannot describe a complex flow. Nevertheless, for lack of a more generally applicable alternative, Eq. (8) has been recommended for estimation of ϵ for process equipment such as stirred tanks (Kresta & Wood, 1993).

In summary, previous methods for turbulent dissipation rate estimation usually involve dubious assumptions and the estimations are rather crude and are seldom space resolved. Direct assessment of the dissipation rate from its definition would require resolution of the fluctuating strain rate tensor, which has been possible only with multiple hot-wire probes. With the advancement of full-field velocimetry techniques, dissipation rate estimation stands to benefit from the availability of spatially resolved instantaneous velocity in a plane, as with particle image velocimetry (PIV) (Keane & Adrian, 1993), or in a volume, as with holographic PIV (HPIV) (Meng & Hussain, 1991, 1995; Barnhart, Adrian & Papen, 1994; Meng, Estevadeordal, Gogineni, Goss & Roquemore, 1997). It is noted that velocity fields provided by PIV are low-pass filtered. In other words, they are resolved to finite scales much like in large eddy simulation. Eddies smaller than the filter width are smoothed out. Furthermore, the low temporal sampling rate of PIV excludes the conventional approach of obtaining spatial information from temporal fluctuations. Hence, conventional dissipation rate approximation methods are not suitable for analyzing PIV data. For this purpose, new methods have to be devised to appropriately use full-field velocity data to estimate dissipation rate.

In this paper, we propose a large eddy-based dissipation rate estimation method using PIV data. The method is demonstrated by estimating the turbulence dissipation rate distribution in the center plane of a stirred vessel. Before we discuss this method in detail, a brief introduction to the large eddy approach is provided below.

1.2. Review of the large eddy approach

To make use of PIV measurements that are limited to finite grid sizes (which often exceed the smallest scales in turbulence when a large global field of view is desired), we borrow the ideas of "large eddy" and "sub-grid scales" from large eddy simulation (LES). In turbulent flows, the large-scale structures are the ones that absorb energy from the mean flow and are strongly flow-dependent. Indeed, these scales tend to be highly anisotropic and vortical in nature, and are responsible for most of the transport in turbulent flows. On the other hand, small-scale structures mainly dissipate the energy provided by larger eddies, and are more universal (i.e., flow-independent) than the large scales. For this reason, large eddy simulation attempts to overcome the limitations of DNS (such as low Reynolds number and simple geometry flows) by resolving only the large scales. The small scales are assumed to be universal and are modeled by sub-grid-scale (SGS) models. Like DNS, LES solves the Navier–Stokes (NS) equations directly for the large scales (Reynolds, 1990; Rogallo & Moin, 1984). The subgrid scales begin at the cutoff wave number, κ_c, chosen to lie in inertial subrange of the energy spectrum. Fig. 1 shows

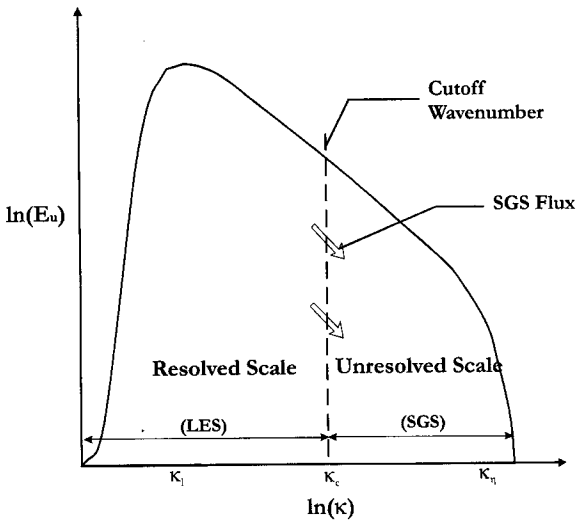

Fig. 1. Schematic model of turbulent kinetic energy transport.

a schematic sketch of the large eddy approach in terms of the energy spectrum. In this figure, κ_l is the integral length scale wave number, and κ_η is the Kolmogorov scale wave number. In LES, a low pass filter (LPF) is applied to the NS equation to separate the resolved scales from the sub-grid scales. In real space, the filtering is defined as a moving spatial average and the bandwidth is defined by $\Delta = 2\pi/\kappa_c$. This filtering process introduces the SGS stress, τ_{ij}, which must be modeled. Several SGS models have been proposed and applied in high Reynolds number simulations, including eddy-viscosity (Smagorinsky, 1963), the similarity model (Bardina, Ferziger & Reynolds, 1984; Liu, Menenveau & Katz, 1994), the gradient model (Clark, Ferziger & Reynolds, 1979; Liu et al. 1994), and various dynamic models (Germano, 1992; Verman, Geurts & Kuerten, 1996).

PIV often uses correlation of double-exposure particle images to extract the velocity field. Since each velocity vector provided by PIV only represents the average velocity over an interrogate cell (IC), the spatial filtering properties of PIV are similar to LES. Therefore, it is more suitable to use a large eddy approach to analyze turbulence characteristics from PIV data than to use traditional methods developed for one-point measurements.

1.3. Review of stirred vessel studies

One of the many flows in which estimation of the turbulence dissipation rate is critical is the stirred vessel. Stirred vessels are some of the oldest and most commonly encountered industrial devices, frequently used in the chemical process industry for gas dispersion in liquids, liquid–liquid blending and solid suspensions in liquids. Understanding flow characteristics such as flow circulation pattern, circulation time, turbulent kinetic energy

distribution, and the turbulence dissipation rate distribution in the tank is crucial. The rate of dissipation is ultimately important in assessing the effectiveness of micro-mixing owing to its close relationship to the smallest scale structures in the flow.

A vast amount of knowledge on the flow characteristics of stirred vessels has been obtained through experimental investigation in recent years (Rao & Brodkey, 1972; Van't Riet & Smith, 1975; Calabrese & Stoots, 1989; Wu & Patterson, 1989; Wu, Patterson & Van Doorn, 1989; Kresta & Wood, 1993; Bakker, Myers, Ward & Lee, 1996; Ward, 1995). Considerable research has been conducted to measure turbulence parameters in this flow, such as the turbulent kinetic energy, length scales and the turbulence dissipation rate. Two different dissipation rates are of interest: the local dissipation rate field (ε) and the average dissipation rate in a finite volume ($\bar{\varepsilon}_v$). Several approximation methods have been proposed to estimate the dissipation rate in stirred tanks from LDV measurements (see Kresta, 1991; Kresta & Wood, 1993; Zhou & Kresta, 1996 for detailed literature review).

Cutter (1966) derived the averaged dissipation rate from a macroscopic energy balance for a Rushton turbine and concluded that turbulent kinetic energy (TKE) is mainly dissipated in the impeller stream ($\sim$ 50%). Wu et al., (1989) used LDV to measure the velocity and turbulent kinetic energy and then performed an energy balance over a defined control volume. They concluded that $\sim$ 30% of energy is dissipated in the discharge stream and $\sim$ 40% is dissipated in the bulk of the vessel. Rao and Brodkey (1972) and Okamoto, Nishikawa and Hashimoto (1981) applied a power spectrum method to stirred tank flows using hot-film and LDV measurements, respectively. Wu and Patterson (1989), Wu et al. (1989); Rao and Brodkey (1972) and Kresta and Wood (1993) estimated the integral length scale by integration of the auto-correlation function. Wu et al. (1989) and Kresta and Wood (1993), further, applied this integral length scale to the dimensional model of dissipation rate (Eq. (7)). Several correction methods have been proposed to adjust characteristic turbulent velocity and length scale (Wu & Patterson, 1989; Wu et al., 1989; Rao & Brodkey, 1972). However, Kresta and Wood (1993) concluded that a sophisticated correction procedure is not necessary. They obtained the characteristic turbulence velocity from the kinetic energy, k, and set $l = W/2$, where W is the width of blade, thereby assuming that the integral length scale is constant throughout the entire vessel. Evidently, all methods proposed in the past to estimate dissipation rate for the stirred vessel in various ways suffer from the limitations of single-point measurements.

In what follows, we introduce the large eddy PIV method for turbulence dissipation rate estimation and apply it to a stirred vessel as an example.

2. The large eddy PIV method

Particle image velocimetry provides spatial information of instantaneous 2D velocity fields simultaneously (see Keane & Adrian, 1993 for a review); hence, spatial derivatives of the velocity fields and spatial covariance can be calculated directly from PIV measurements without Taylors hypothesis or isotropic turbulence assumptions. However, the spatial resolution of PIV is limited. It can be represented by

$$L_r = \frac{L_{IC}}{L_{CCD}} \cdot L_v \,, \tag{9}$$

where L_r is the smallest resolved length scale with the PIV system, L_v the length scale of the viewing area in the flow, and L_{IC} and L_{CCD} the dimensions of the interrogation cell (IC) and CCD array, respectively (usually in number of pixels). Clearly, for a given PIV technique, the decrease of L_r, requires the reduction of the viewing area size L_v. For a typical PIV system where $L_{IC} = 32$ pixels and $L_{CCD} = 1024$ pixels, and a flow at $\mathrm{Re} = 10^6$ based on the integral length scale of 10 cm, the viewing area dimension of the PIV measurement is only 0.1 mm in order to resolve the Kolmogorov scale (3 μm). This field of view is usually too small to provide useful full field information for chemical process applications. The alternative is to sacrifice spatial resolution.

It must be further noted that the velocities from PIV measurements are different in nature from velocities obtained by single-point velocimetry techniques. As a result of the correlation technique (which generally forms the basis of PIV data reduction), each velocity vector is a result of a spatial average of the velocity field in one IC. In other words, it is low-pass filtered. Care must be taken when statistical quantities such as time-averaged mean velocity, turbulence kinetic energy, and Reynolds stresses are extracted from PIV data. The real, point-wise velocity can be written in terms of the PIV resolved (spatially averaged) velocity:

$$u_i = \bar{U}_i - \Phi(\bar{U}_i) + \tfrac{1}{2!}\Phi^2(\bar{U}_i) - \tfrac{1}{3!}\Phi^3(\bar{U}_i) + \ldots \,, \tag{10}$$

where $\Phi(\bar{U}_i) = (a_1\partial^2/\partial x_1^2 + a_2\partial^2/\partial x_2^2 + a_3\partial^2/\partial x_3^2)\bar{U}_i$, $\bar{U}_i$ is the PIV resolved velocity, and a_1, a_2, a_3 are constants related to the low-pass filter bandwidths for each direction. For a uniform filter, the constants are defined as

$$a_i = \frac{\Delta_i^2}{8} \,, \quad i = 1, 2, 3, \tag{11}$$

where Δ_i is the filter width along the ith axis. For an isotropic filter, filter widths along all three axes are the same, denoted as Δ. Therefore, Eq. (10) can be rewritten as

$$u_i = \bar{U}_i - \frac{\Delta^2}{8} L^2 \bar{V}_i + \frac{\Delta^4}{1024} \nabla^4 \bar{U}_i + \ldots \,. \tag{12}$$

Based on dimension analysis, the second term in Eq. (12) scales like Δ^2/l^2, where l is the local integral length scale. Therefore, the true velocity, u_i, can be approximated by PIV measurement $\bar{U}_i$ when $\Delta \ll l$. In this limit, the following relationships hold

$$\langle u_i \rangle \approx \langle \bar{U}_i \rangle , \tag{13}$$

$$u_i' \approx \bar{U}_i - \langle \bar{U}_i \rangle , \tag{14}$$

$$\langle u_i' u_j' \rangle \approx \bar{U}_i \bar{U}_j - \langle \bar{U}_i \rangle \langle \bar{U}_j \rangle . \tag{15}$$

Here, brackets represent ensemble average. Hence, when the IC size is much smaller than the local integral scale of the flow, Reynolds-averaged statistical quantities can be approximated from PIV data.

For high Reynolds number flows, the turbulent kinetic energy is generated at (flow-dependent) large scales and cascades to (universal) small scales where it dissipates in the viscous sub-range. By examining the production and dissipation as a function of the wave number (Fig. 2), it can be shown that the turbulent kinetic energy is mainly generated at the integral scale, and then the same amount of energy is dissipated near the Kolmogorov scale. In between, there is a large region (inertial subrange) where turbulent kinetic energy is neither generated nor dissipated. The major role of turbulent structures in the inertial sub-range is thus to transfer energy from large to small-scale structures without change. Hence, when the sub-integral scales are in dynamic equilibrium, the flux of turbulent kinetic energy through the inertial sub-range will be equal to the turbulence dissipation rate.

Based on this physical model, we propose to estimate the turbulent kinetic energy transferred from large to small scales, and thus, to approximate the turbulence dissipation rate. Since only the length scales within the inertial sub-range are needed to estimate the flux of turbulent kinetic energy, the proposed method does not require the velocity field to be resolved down to the Kolmogorov scale. Therefore, it can provide a direct estimation of the dissipation rate over rather large flow regions. A mathematical description of the method is provided below.

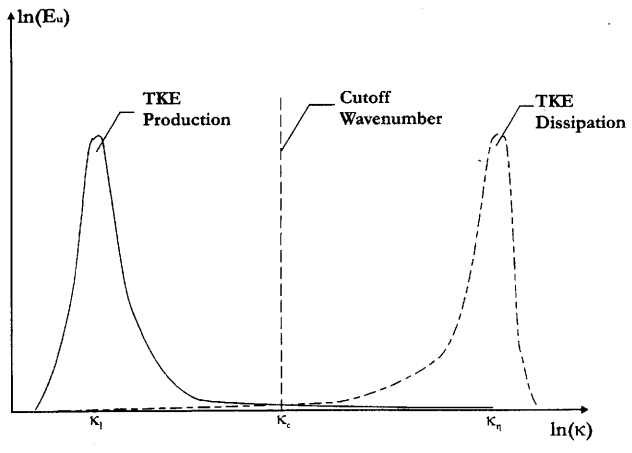

Fig. 2. Schematic model of production and dissipation of turbulent kinetic energy.

The instantaneous velocity, u_i, and pressure, p_i, can be written as

$$\begin{aligned} u_i &= \bar{U}_i + \breve{u}_i , \\ p_i &= \bar{P}_i + \breve{p}_i , \end{aligned} \tag{16}$$

where $\bar{U}_i$, $\bar{P}_i$ are the resolved-scale velocity and pressure, respectively, found by PIV measurements, and $\breve{u}_i$, $\breve{p}_i$ are the unresolved-scale velocity and pressure. By filtering the incompressible continuity equation and the Navier-Stokes equation, the LES equations are obtained:

$$\frac{\partial \bar{U}_i}{\partial x_i} = 0, \tag{17a}$$

$$\frac{\partial \bar{U}_i}{\partial t} + \frac{\partial (\bar{U}_i \bar{U}_j)}{\partial x_j} = -\frac{\partial \bar{P}}{\partial x_j} + \upsilon \frac{\partial^2 \bar{U}_i}{\partial x_j^2} - \frac{\partial \tau_{ij}}{\partial x_j} , \tag{17b}$$

where $\tau_{ij} = \overline{u_i u_j} - \bar{U}_i \bar{U}_j$ is the SGS stress tensor, which must be modeled by a sub-grid-scale (SGS) turbulence model. Multiplying Eq. (17b) by $\bar{U}_i$ and contracting, the resolved-scale kinetic energy transport balance equation is obtained:

$$\frac{\partial \bar{q}^2}{\partial t} + \bar{U}_j \frac{\partial \bar{q}^2}{\partial x_j} = \frac{\partial}{\partial x_j} \left(-\bar{P}\bar{U}_j + \upsilon \frac{\partial \bar{q}^2}{\partial x_j} - \tau_{ij} \bar{U}_i \right) - \upsilon \frac{\partial \bar{U}_i}{\partial x_j} \frac{\partial \bar{U}_i}{\partial x_j} + 2\tau_{ij} \bar{S}_{ij} , \tag{18}$$

where $\bar{S}_{ij}$ is the resolved scale strain rate tensor defined by

$$\bar{S}_{ij} = \frac{1}{2} \left(\frac{\partial \bar{U}_j}{\partial x_i} + \frac{\partial \bar{U}_i}{\partial x_j} \right) . \tag{19}$$

The last term in Eq. (18) is the eddy dissipation, which models the kinetic energy transported to small scales from the resolved scales. According to our previous argument, this term will be equal to the turbulent kinetic energy dissipated in the smallest scales. Therefore, the turbulence dissipation rate can be approximated by computing the Reynolds averaged SGS dissipation rate

$$\varepsilon \approx \langle \varepsilon_{SGS} \rangle = -2 \langle \tau_{ij} \bar{S}_{ij} \rangle , \tag{20}$$

where, in practice, the Reynolds average on the right-hand side is replaced by a time average over sequential full-field PIV data sets. Eq. (20) embodies the essence of the large-eddy PIV method. Under the dynamic equilibrium assumption, the turbulence dissipation rate ε can be estimated by the SGS energy flux ε_{SGS} at the cut-off scale corresponding to the PIV resolution. The SGS flux is obtained from the strain-rate tensors, $\bar{S}_{ij}$, computed from

the PIV measured (resolved) velocity fields and the modeled SGS stress, τ_{ij}. When the PIV system resolves down to the Kolmogorov scale, the SGS stress is replaced with the viscous shear stress. In other words, the resolved velocity fields directly give the dissipation rate.

The SGS stress τ_{ij} in Eq. (20) has to be closed by a model. Various SGS models have been proposed in the literature:

1. *Smagorinsky model*: The eddy viscosity model (Smagorisky, 1963) is given by

$$\tau_{ij} = -C_s^2 \Delta^2 |\bar{S}| \bar{S}_{ij}, \tag{21}$$

where $C_s = 0.17$ is the Smagorinsky constant. This value will be adopted in our analysis. Based on LES simulations of Eq. (17a) and (17b), the Smagorinsky model has been found to be too dissipative in laminar regions with mean shear. However, we expect the model to give good results in high Reynolds number turbulent flows.

2. *Similarity model*: The similarity model (Liu et al., 1994) is based on the assumption that the velocities at different scales give rise to turbulent stresses with similar structures. The model can be expressed as

$$\tau_{ij} = \overline{\bar{u}_i \bar{u}_j - \bar{u}_i \bar{u}_j}. \tag{22}$$

In contrast to the eddy-viscosity model, this model has a mechanism to represent backscatter of energy for SGS to resolved scales. Since, in practice, the double filtered velocity correlation (first term in Eq. (22)) is not available from experimental measurement, the similarity model is unsuitable for dissipation rate estimation.

3. *Gradient model*: Clark et al. (1979) modeled the SGS stress as an inner product of the velocity gradients

$$\tau_{ij} = \frac{1}{12} \Delta^2 \left(\frac{\partial \bar{U}_i}{\partial x_k}\right)\left(\frac{\partial \bar{U}_j}{\partial x_k}\right). \tag{23}$$

This model is equal to the similarity model expanded in a low-order Taylor series (Liu et al., 1994), and ensures forward scatter and backscatter of energy between resolved scale and SGS. Since all the terms are measured from the resolved velocity field, this model is suitable for the proposed dissipation rate estimation.

4. *Dynamic model*: In order to overcome the shortcomings of Smagorinsky model, the model constant, C_s, is replaced by a coefficient obtained dynamically, depending on the local structure of the resolved fields. Since the dynamic coefficient is not available from experimental measurement, the dynamic model is unsuitable for use with PIV data.

In this paper, these SGS models will be used to estimate the turbulence dissipation rate from PIV data using Eq. (20).

3. Estimation of the dissipation rate in a stirred vessel

The large-eddy PIV method is applied to a pitched blade turbine (PBT) stirred vessel. This work is based on a study by Sheng, Meng and Fox (1998), who attempted to validate CFD simulation results (including turbulence dissipation rate) using PIV measurements.

3.1. PIV Experiment

The PIV experiment has been described in detail by Ward (1995) and reported by Bakker et al. (1996). The axial impeller stirred vessel was a Plexiglas circular water tank of diameter $T = 0.292$ m with the fluid height maintained at 0.311 m. Four axial baffles (width = 0.0243 m) were mounted along the wall as shown in Fig. 3. A P-4 impeller of diameter $D = 0.102$ m with 45° pitch was located at a height $C = 0.134$ m from the bottom. The ratio between the vessel and the impeller diameter was $D/T = 0.35$ and the off bottom clearance was $C/T = 0.46$. The ratio of blade width (W) to the impeller diameter (D) was 0.20. The impeller was driven at 60 rpm, resulting in a Reynolds number of about 9200 based on impeller diameter and the tip velocity. The integral length scale of a stirred tank is often taken as half of the impeller width, since it is approximately the size of the trailing vortices (Kresta & Wood, 1993). Following this convention, the integral length scale is $l = 10$ mm.

The PIV system was a Dantec Flowgrabber™ owned by Chemineer, Inc. An argon-ion laser was used to produce a 10 mm thick light sheet, which illuminated the

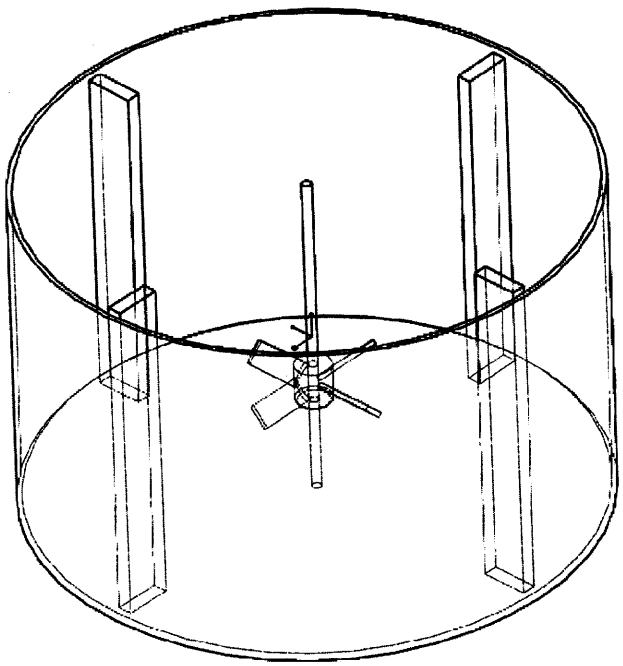

Fig. 3. Sketch of the stirred vessel with a pitched P-4 impeller used for the PIV experiments.

tank from the top. To compensate for the refractive index variation, the circular tank was kept inside a square tank filled with a compensating liquid. An 8-bit, black-and-white 512×480 CCD camera was used to acquire particle images. The viewing area of the camera was set to cover the entire vessel. The flow was seeded with 0.1 g of neutrally buoyant 80 μm diameter fluorescent polymer spheres, resulting in a seeding density of 15–25 particles in a 16×16 pixel sampling window. The continuous-wave laser was shuttered to produce 10 μs of exposure. Two consecutive images were cross-correlated to give the velocity field. A total of 59×50 vectors were given for the entire plane at each instant on a non-uniform grid. A total of 1024 instantaneous 2D velocity field measurements were carried out over a period of 22 min with a sampling rate of 0.77 Hz. Since the overall viewing area is large (whole tank), the average spatial resolution of the vectors is limited to roughly 5 mm. Hence the resolved scale is much larger than the Kolmogorov length scale $\eta = 10$ μm. This clearly calls for the large eddy PIV approach.

The PIV measurement accuracy is analyzed as follows. Errors in spatial derivatives of velocity result from the velocity (displacement) measurement and spatial differentiation. With sub-pixel resolution implemented in Dantec's FFT-based correlation software, the particle displacement estimation error is 0.1 pixel over 8 pixels or 1.25%, where an IC size of 16×6 is adopted. The spatial derivative error would be 1 pixel over 16 pixels or 6.25% if a direct finite difference method is used. Hence, the total error in a velocity derivative would be 7.5%. The dissipation rate contains multiple products of velocity derivatives, and hence would suffer an error of multiple times of 15%, which is clearly unacceptable. Hence, to obtain velocity derivatives and especially to estimate dissipation rate using PIV, it is imperative to cut down the derivative errors and also to reduce the PIV measurement errors. For this reason, in the current work we employ an adaptive-window derivative scheme. In this scheme, the resolved velocity field is interpolated by the cubic-spline method, and then a central difference scheme over an adaptive window is applied to calculate the derivatives. As long as the interpolation can faithfully resolve the velocity field (which is a fairly good assumption), the resolution of the derivatives reaches 10^{-4}. Hence, the spatial differentiation error is negligible and the remaining error in our velocity derivatives is only the PIV velocity measurement error, 1.25%. This error can be further reduced by adopting larger IC window sizes; for example, 32×32 or 64×64 are commonly used, resulting in improved accuracy of 0.6% and 0.3%, respectively.

It should be pointed out that, besides correlation, there are other methods to extract velocity fields from PIV images, such as particle tracking and particle pairing. However, these techniques are less widely used than FFT-based correlation method.

3.2. Analysis of PIV experimental data

To estimate the dissipation rate from PIV measurements using the large-eddy PIV method and other methods for comparison, we evaluate if the premises of these methods are satisfied. First, we check if the higher-order terms in Eq. (12) can be dropped so that the statistical quantities can be calculated from the resolved scale velocity, $\bar{U}_i$, using the relationships given in Eqs. (13)–(15). The average filter width (equal to the IC size) for the PIV measurement here is $\Delta = 5$ mm while the integral scale is $l \approx 10$ mm. Thus, the second term in Eq. (12) is one order of magnitude smaller than the first term. Second, we roughly check if the dynamic equilibrium assumption holds. As pointed out before, the Kolmogorov length scale, estimated from the Reynolds number based on the integral length scale of $l \approx 10$ mm is $\eta \approx 10$ μm. Between η and l there is a large region within which the cut-off scale $L_c = 5$ mm lies. We thus assume that the conditions for approximating the dissipation rate by the large-eddy PIV method are satisfied.

Some treatments are necessary to circumvent the 2D limitation of PIV. Below are two situations where such simplifications are made in our data processing.

First, for comparison purposes, we will compute the dissipation rate using the dimensional argument, Eq. (8). This requires the turbulent kinetic energy $k = \frac{1}{2}\langle(\bar{U}_i - \langle\bar{U}_i\rangle)^2\rangle$ to be obtained from PIV. Since the PIV data only contain the axial and radial components, the circumferential normal stress will be approximated from the axial and radial normal stresses by assuming the flow to be locally isotropic at the resolved scales. The turbulent kinetic energy is thus estimated from

$$k = \frac{3}{4}\sum_{i=1}^{2}\langle(\bar{U}_i - \langle\bar{U}_i\rangle)^2\rangle . \tag{24}$$

Second, in order to evaluate the dissipation rate using Eq. (20), a total of nine components of the strain rate tensor in Eq. (19) have to be measured. Currently PIV can only provide five out of the nine components: two off-diagonal and three diagonal components (directly measured and derived from the continuity equation). What are missing from direct PIV measurements are the derivatives of circumferential velocity and derivatives with respect to the circumferential axis

$$\frac{\partial\bar{W}}{\partial x}, \frac{\partial\bar{W}}{\partial y}, \frac{\partial\bar{W}}{\partial z}, \frac{\partial\bar{U}}{\partial z}, \frac{\partial\bar{V}}{\partial z} .$$

Due to large-scale anisotropic motion in this flow, the missing strain-rate covariance cannot be approximated from the known terms theoretically. However, examination of the five known components of dissipation rate tensor (using the Smagorisky model) reveals that, they all have similar distributions and magnitudes (Figs. 4a–d).

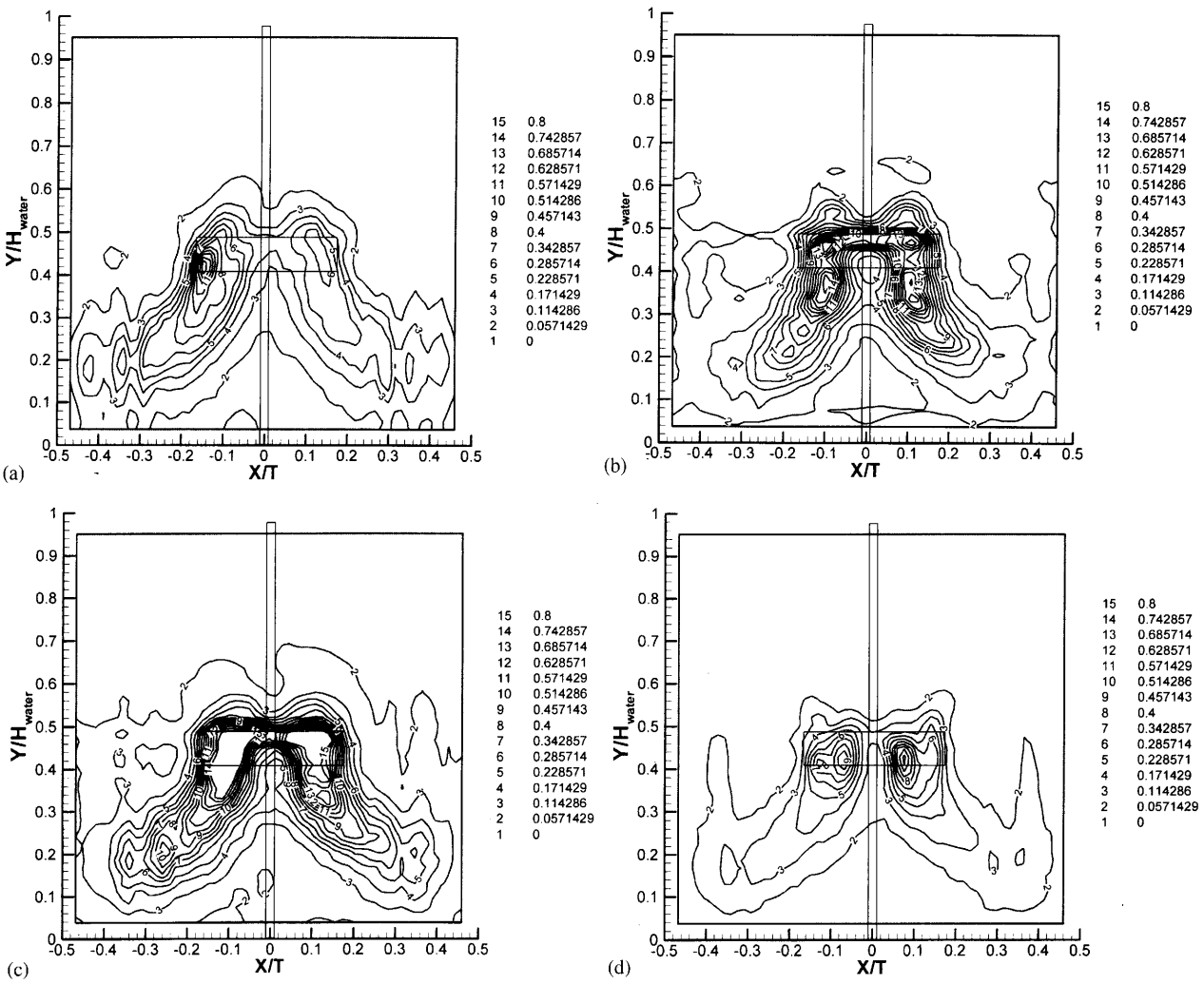

Fig. 4. Components of the dissipation rate tensor (a)ε_{11} (b)ε_{22} (c)ε_{33} (d) $\varepsilon_{12} = \varepsilon_{21}$.

We thus assume that the dissipation rate can be approximated by multiplying the sum of the known components by a factor of 9/5. Obviously, further improvement of the dissipation rate approximation will require extension of the velocity measurement to 3D.

3.3. Dissipation rate and comparison

Figs. 5 and 6 show the dissipation rate calculated using the large-eddy PIV approach, where the SGS stress is obtained from Smagorinsky and the Gradient models, respectively. A high dissipation region is evident from both figures around the impeller and in the flow discharge regions, overlapping with the strong shear layer in the mean velocity flow field (Fig. 7). To illustrate the similarity between these two ϵ distributions, their cross-correlation distribution is plotted in Fig. 8. It is observed that the cross-correlation coefficient lies between 0.97 and 0.99. Calculations of the SGS stress using the other models given in the introduction yielded similar results, that is, these dissipation rate estimations agree with each other in magnitude as well as in spatial distribution. Hence, it can be concluded that the choice of the SGS model is not important in the large-eddy PIV method.

To compare these results with the dimensional analysis method, Eq. (8) is employed using the PIV data and constants $l = 10$ mm (half the impeller width) and $A = 1$. The estimated dissipation rate is shown in Fig. 9. As far as the shape of distribution is concerned, the large eddy estimations (Figs. 5 and 6) correspond reasonably well with the dimensional analysis result. Both estimations show a focused high-dissipation region at the impeller and flow discharge regions. Moreover, both provide a maximum to minimum dissipation rate ratio of 10, which suggests that the dissipation rate distribution in the stirred tank is highly inhomogeneous. However, the dissipation rate obtained by dimensional analysis has much larger values in the bulk of the vessel than those

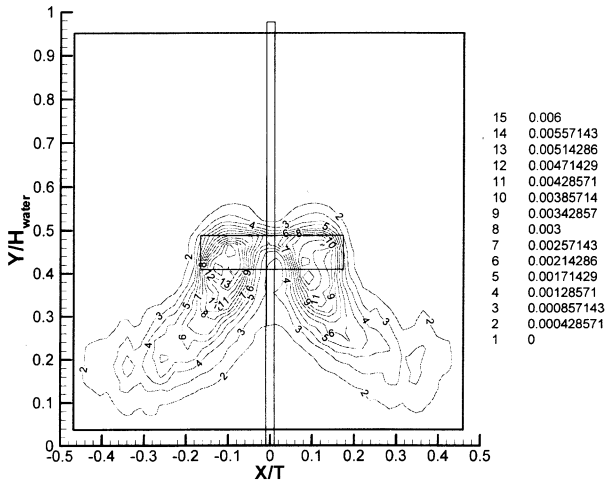

Fig. 5. Dissipation rate, ε, for the flow in a stirred tank by modeling the SGS flux using the Smakorinsky eddy-viscosity model.

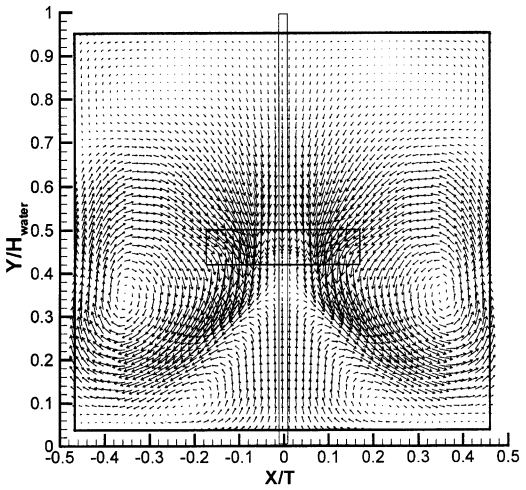

Fig. 7. Mean velocity field produced by a P-4 impeller obtained by PIV.

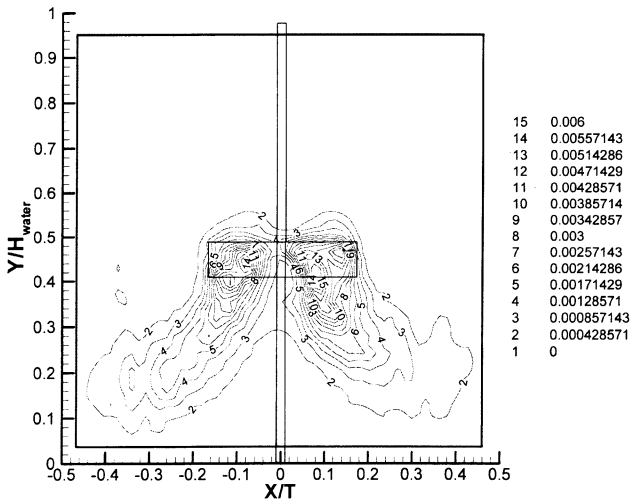

Fig. 6. Dissipation rate, ε, for the flow in a stirred tank by modeling the SGS flux using the Gradient model.

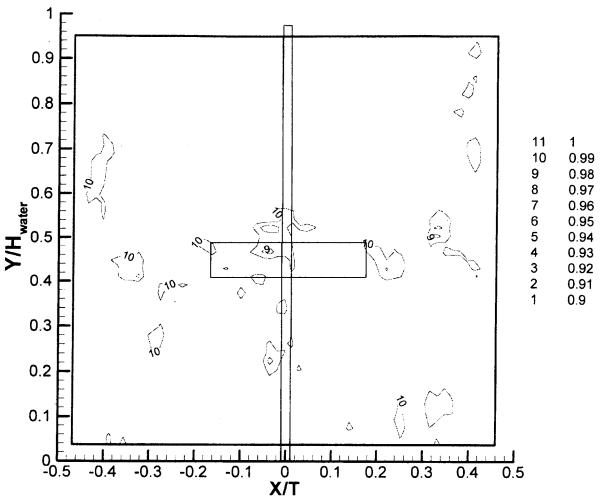

Fig. 8. Cross-correlation coefficient (co-variance) distribution of estimations by the Smakorinsky model and the Gradient model.

found by the large eddy approach. Fig. 10 shows the cross-correlation distribution of the large-eddy estimation obtained by the Smagorisky model with that from dimensional analysis. Large discrepancies are evident in the bulk of the tank. This discrepancy is most likely a result of the assumption employed by the dimensional analysis method, that the integral length scale in the bulk of tank is the same as in the impeller region. Indeed, one would expect the local integral length scale to be significantly smaller near the impeller than in the bulk fluid. This behavior is seen in Fig. 11, which shows the integral length scale distribution ($l = k^{3/2}/\varepsilon$) in the stirred tank, where k and ε are computed from the large-eddy approach.

Dissipation rates averaged in the impeller and flow discharge regions as a percentage of the total dissipation rate in the tank have been computed by integrating the local dissipation rate over a finite area in 2D. Table 1 shows the results obtained for the three different estimation methods and those reported by Cutter (1966), Wu and Patterson (1989), and Jaworski and Fort (1991). From the table, one can see that the results obtained with the large-eddy method agree with most reported results rather well for this flow. On the other hand, the average dissipation rate in the impeller region is underestimated by the dimensional analysis method.

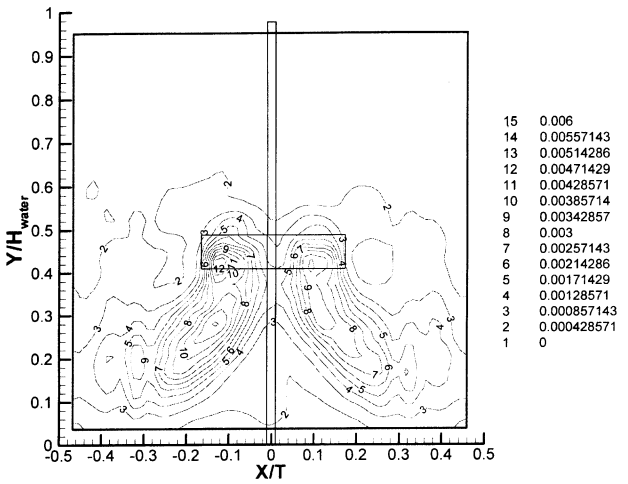

Fig. 9. Dissipation rate, ε, for the flow in a stirred tank using dimensional analysis method formula, where constant A is 1, integral length scale is $D/10$, and characteristic fluctuating velocity is obtained from turbulent kinetic energy, k.

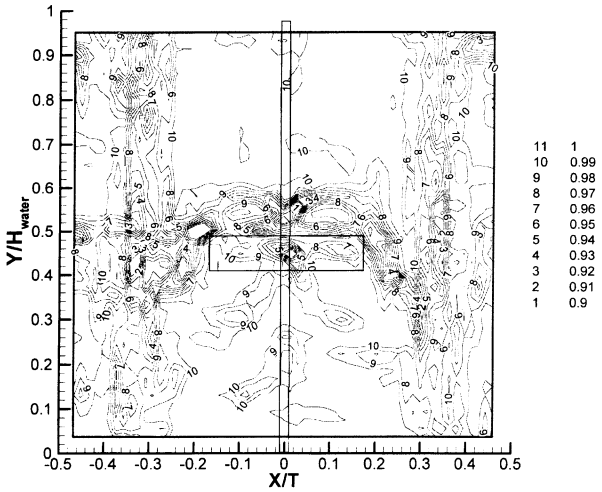

Fig. 10. Cross-correlation coefficient distribution of ε estimations by large-eddy approach (with Smakorinsky model) and by dimensional analysis method.

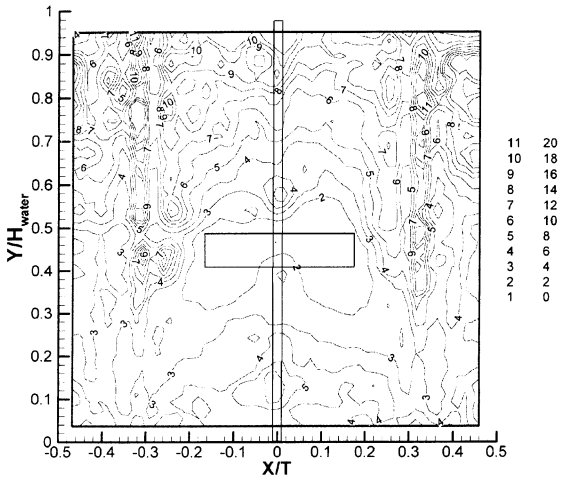

Fig. 11. Normalized integral length scale in the stirred tank, calculated by $l = k^{3/2}/\varepsilon$ and normalized with the half of blade width ($W/2$).

Table 1
Comparison of the dissipation rate averaged in the impeller region and flow discharge region as a percentage of the total dissipation rate in the tank

	Dissipation rate averaged in impeller region (%)	Dissipation rate averaged in flow discharge region (%)
Large-eddy PIV approach using Smagorinsky model	30	48
Large-eddy PIV approach using the Gradient model	30	47
Dimensional argument by Kresta and Wood (1993)	15	45
Cutter (1966)	20	50
Wu and Patterson (1989)	30	40
Jaworski and Fort (1991)	32	54

4. Conclusions and discussions

In this paper, we propose a dissipation rate estimation technique based on a large-eddy PIV approach. The basis for using PIV measurements is that: (i) From PIV, the velocity field in a plane is simultaneously obtainable, lending itself to spatial derivative calculation. (ii) PIV measurements usually do not resolve to the smallest turbulent eddies, and they do not have to (hence the need for a "large-eddy" approach). (3) Some terms in the dissipation estimation are unavailable if PIV provides only two components, as is usually true at the present stage. However, the missing terms can be approximated from available terms, and this procedure involves far less dubious assumptions than most other methods of dissipation rate estimation. The basic idea of the large-eddy estimation method lies in the dynamic equilibrium assumption, which is usually valid at high Reynolds numbers. The total energy dissipated at the smallest scale, ε, is approximated by the sub-grid scale energy flux, ε_{SGS}, from the resolved scale to the sub-grid scale. The SGS flux is obtained from the strain-rate tensors computed from PIV velocity fields and the modeled SGS stress. When the PIV measurement resolves down to the Kolmogorov scale, the SGS stress is replaced with the viscous shear stress. In other words, the resolved velocity fields directly give the dissipation rate.

The proposed method is applied to estimation of dissipation rate distribution in a stirred tank with an axial impeller using PIV data with the full-tank viewing area

and a coarse spatial resolution of 5 mm. Two different SGS models, Smagorinsky eddy-viscosity and gradient model, are employed in the estimation of SGS stress, yielding consistent results. The computed dissipation rate distributions are compared with results obtained using the dimensional analysis method employed by Kresta and Wood (1993). All three estimations, based on the same PIV measurements, agree with each other rather well. However, the large-eddy PIV method is inherently more accurate for inhomogeneous and anisotropic flows. Furthermore, the use of PIV measurements enables the dissipation rate distribution to be estimated over a large area.

Beyond the current work, further research is needed to address the following questions:

First, our physical model implicitly assumes the dynamic equilibrium, wherein the turbulent kinetic energy SGS flux is equal to the dissipation rate. This enables us to approximate the turbulence dissipation rate by measuring total kinetic energy flux from the resolved to the unresolved scale (the SGS flux). For non-equilibrium turbulence such as rapid distortion, however, this assumption is challenged. We think that at least some correction must be introduced to the SGS flux to compensate for the local loss. How to make this correction is an open problem. Furthermore, like all turbulence models, the models used to account for the SGS stress, τ_{ij}, lack physical meaning.

Second, from the derivation of Eq. (20), it is clear that the accuracy of our approximation highly depends on the filter bandwidth, and thus, the interrogation cell size in PIV. The choice of PIV configuration has to be carefully evaluated in light of the anticipated turbulence length scales, especially the integral and Kolmogorov length scales.

Lastly, the direct measurement of the dissipation rate requires the ability to measure all of the terms in Eqs. (1) and (2). Since the current PIV technique lacks the capability tomeasure 3D velocity fields, the circumferential velocity component is missing; therefore, its derivatives and all derivatives along the circumferential direction are lacking. The effect of these missing terms in the strain rate tensor on the estimation cannot be accurately evaluated due to anisotropicity of the flow at the resolved scale. Furthermore, data resolved on a 2D plane in a vastly 3D flow provide, at most, very limited insight into the dynamics of complex flows. Clearly, fully resolved 3-component velocity measurements in a 3D volume as a function of time are strongly needed. Hence, it is essential to develop 3D PIV techniques such as stereoscopic PIV (Adrian, Soloff, Liu, Meinhart & Lai, 1997), Particle Tracking Velocimetry (Guezennec, Brodkey & Kent, 1994) and Holographic PIV (Meng & Hussain, 1991, 1995; Barnhart et al., 1994; Meng et al., 1997). Among these, the holographic PIV gives instantaneous 3D volumetric recording and provides the highest spatial resolution, and hence is the most promising technique.

Notation

A	dimensional analysis constant
C	impeller off-bottom clearance
C_s	Smagorisky model constant
D	impeller diameter
E_1	one-dimensional power spectrum
K	turbulent kinetic energy
l	integral length scale
L_{IC}	dimension of interrogation cell
L_{CCD}	dimension of CCD sensor size
L_V	dimension of camera viewing area
L_c	cutoff length scale
p'	pressure fluctuation
$\check{p}$	unresolved-scale pressure
P	instantaneous pressure
$\langle p \rangle$	time-averaged instantaneous pressure
$\bar{P}$	filtered pressure in time or space domain
$\bar{q}^2$	resolved-scale kinetic energy
s'_{ij}	fluctuating strain rate tensor
$\bar{S}_{ij}$	filtered strain-rate tensor in time or space domain
t	time
T	tank diameter
u'_i	fluctuating velocity
u_i	instantaneous velocity
$\langle u_i \rangle$	time-averaged instantaneous velocity
$\check{u}_i$	unresolved-scale velocity
$\bar{U}_i$	filtered velocity components in time or space domain
W	impeller blade width
x_I	x, y, and z coordinates

Greek letters

Δ	filter width for an isotropic spatial filter
Δ_i	filter width along the ith axis
ε	turbulence dissipation rate
ε_{SGS}	sub-grid scale flux
$\bar{\varepsilon}_v$	average dissipation rate in a finite volume
η	Kolmogorov length scale
κ	wave number
κ_c	cut-off wave number
κ_l	integral scale wave number
κ_η	Kolmogorov scale wave number
λ	Taylor micro-scale
μ	molecular viscosity
υ	kinematic viscosity
τ_{ij}	sub-grid scale stress

Acknowledgements

The authors wish to thank A. Bakker of Chemineer, Inc., K. J. Myers, R. W. Ward of University of Dayton for providing the PIV measurement data in the stirred vessel used in this study. Support from National Science Foundation through grants CTS-9625307 (HM) and

CTS-9158124 (ROF), and a matching grant from the Dow Chemical Company for the development and application of holographic PIV are greatly appreciated. We would also like to acknowledge R. S. Brodkey for helpful discussions on PTV data analysis. The work was performed at the Kansas State University.

References

Adrian, R. J., Soloff, S. M., Liu, Z., Meinhart, C. D., & Lai, W. (1997). Stereoscopic PIV applications to the study of turbulence. *Proceedings of the second international workshop on PIV'97-Fukui*, Japan (pp. 75–84).

Andreopoulos, Y., & Honkan, A. (1996). Experimental techniques for highly resolved measurements of rotation, strain, and dissipation-rate tensors in turbulent flows. *Measurement in Science and Technology*, *7*, 1462–1476.

Batchelor, G. K. (1953). *The Theory of Homogeneous Turbulence*. Cambridge, MA: Cambridge University Press.

Bakker, A., Myers, K. J., Ward, R. W., & Lee, C. K. (1996). The laminar and turbulence flow pattern of a pitched blade turbine. *Transactions of the Institution of Chemical Engineers*, *74*, 485–491.

Bardina, J., Ferziger, J. H., & Reynolds, W. C. (1984). *Improved turbulence models based on LES of homogeneous incompressible turbulence flows*. Rep. TF-19 Dept. of Mechanical Engineering, Stanford.

Barnhart, D. H., Adrian, R. J., & Papen, G. C. (1994). Phase-conjugate holographic system for high resolution particle image velocimetry. *Applied Optics*, *33*, 7159–7170.

Calabrese, R. V., & Stoots, C. M. (1989). Flow in the impeller region of a stirred tank. *Chemical Engineering Progress*, *85*, 43–50.

Clark, R. A., Ferziger, J. H., & Reynolds, W. C. (1979). Evaluation of subgrid-scale models using an accurately simulated turbulent flow. *Journal of Fluid Mechanics*, *91*, 1–16.

Cutter, L. A. (1966). Flow and turbulence in a stirred tank. *A.I.Ch.E. Journal*, *12*, 35–45.

Germano, M. (1992). Turbulence: The filtering approach. *Journal of Fluid Mechanics*, *238*, 325–336.

Guezennec, Y. G., Brodkey, R. S., & Kent, J. C. (1994). Algorithms for fully automated three-dimensional particle tracking velocimetry. *Experiments in Fluids*, *17*, 209–213.

Hinze, J. O. (1994). *Turbulence*. New York: McGraw-Hill, Inc.

Hussein, H. J., & Martinuzzi, R. J. (1995). Energy balance for turbulence flow around a surface mounted cube placed in a channel. *Physics of Fluids*, *8*, 764–780.

Jaworski, Z., & Fort, I. (1991). Energy dissipation rate in a baffled vessel with pitched blade turbine impeller. *Collection of Czechoslovak Chemical Communications*, *56*, 1856–1867.

Keane, R. D., & Adrian, R. J. (1993). Theory and simulation of particle image velocimetry (Invited Lecture). *Laser Anemometry, Advances and Applications*, *5*, 477.

Kresta, S.M. (1991). *Measurement, characterization, and prediction of the turbulent flow in stirred tanks. PhD Thesis*, McMaster University, Hamilton, Ontario.

Kresta, S. M., & Wood, P. E. (1993). The flow field produced by a pitched blade turbine: characterization of the turbulence and estimation of the dissipation rate. *Chemical Engineering Science*, *48*, 1761–1774.

Landahl, H. T., & Mollo-Christensen, E. (1992). *Turbulence and random processes in fluid mechanics*. Cambridge, MA: Cambridge University Press.

Liu, S., Menenveau, C., & Katz, J. (1994). On the properties of similarity subgrid-scale models as deduced from measurements in a turbulence jet. *Journal of Fluid Mechanics*, *275*, 83–119.

Meng, H., Estevadeordal, J., Gogineni, S., Goss, L., & Roquemore, W. M. (1997). Holographic flow visualization as a tool for studying 3D coherent structures and instabilities. *Proceedings of the second international workshop on PIV'97-Fukui*, Japan (pp. 27–34).

Meng, H., & Hussain, F. (1991). Holographic particle velocimetry, a 3D measurement technique for vortex interactions, coherent structures and turbulence. *Fluid Dynamics Research*, *8*, 33–52.

Meng, H., & Hussain, F. (1995). In-line recording and off-axis viewing technique for holographic particle velocimetry. *Applied Optics*, *34*, 1827–1840.

Okamoto, Y., Nishikawa, N., & Hashimoto, K. (1981). Energy dissipation rate distribution in mixing vessels and its effects on liquid-liquid dispersion and solid-liquid mass transfer. *International Chemical Engineering*, *21*, 88–94.

Rao, M. A., & Brodkey, R. S. (1972). Continuous flow stirred tank turbulence parameters in the impeller stream. *Chemical Engineering Science*, *27*, 137–156.

Reynolds, W. C. (1990). The potential and limitations of direct and large eddy simulations. *Whither Turbulence? Turbulence at the Crossroads*, *15*, 313–343.

Rogallo, R. S., & Moin, P. (1984). Numerical simulation of turbulent flow. *Annual Review of Fluid Mechanics*, *16*, 99–137.

Sheng, J., Meng, H., & Fox, R. O. (1998). Validation of CFD simulations of a stirred tank using Particle Image Velocimetry data. *Canadian Journal of Chemical Engineering*, *76*(3), 711–725.

Smagorinsky, J. (1963). General circulation experiments with the primitive equation I the basic experiment. *Monthly Weather Review*, *91*, 99–164.

Tennekes, H., & Lumley, J. L. (1972). *A First Course in Turbulence*. Cambridge, MA: MIT Press.

Van't Riet, K., & Smith, J. M. (1975). The trailing vortex system produced by Rushton turbine agitators. *Chemical Engineering Science*, *30*, 1093–1105.

Verman, B., Geurts, B., & Kuerten, H. (1996). Large Eddy simulation of the temporal mixing layer using the Clark model. *Theoretical Computations in Fluid Dynamics*, *8*, 309–324.

Ward, R.W. (1995). *A DPIV investigation of flow pattern instabilities of axial-flow impellers. MSc. Thesis*, University of Dayton.

Wu, H., Patterson, G. H., & Van Doorn, M. (1989). Distribution of turbulence energy dissipation rates in a Rushton turbine stirred mixer. *Experiments in Fluids*, *8*, 153–160.

Wu, H., & Patterson, G. K. (1989). Laser doppler measurements of turbulent flow parameters in a stirred mixer. *Chemical Engineering Science*, *44*, 2207–2221.

Zhou, G., & Kresta, S. M. (1996). Distribution of energy between convective and turbulence flow for three frequently used impellers. *Collection of Czechoslovak Chemical Communications*, *74*, 379–389.